

Mechanical alloying and theoretical studies of MnAl(C) magnets

Van Tang Nguyen, Florent Calvayrac, Anna Bajorek, Nirina Randrianantoandro

▶ **To cite this version:**

Van Tang Nguyen, Florent Calvayrac, Anna Bajorek, Nirina Randrianantoandro. Mechanical alloying and theoretical studies of MnAl(C) magnets. Journal of Magnetism and Magnetic Materials, 2018, 462, pp.96-104. 10.1016/j.jmmm.2018.05.001 . hal-01906072

HAL Id: hal-01906072

https://univ-lemans.hal.science/hal-01906072

Submitted on 17 Dec 2018

HAL is a multi-disciplinary open access archive for the deposit and dissemination of scientific research documents, whether they are published or not. The documents may come from teaching and research institutions in France or abroad, or from public or private research centers.

L'archive ouverte pluridisciplinaire **HAL**, est destinée au dépôt et à la diffusion de documents scientifiques de niveau recherche, publiés ou non, émanant des établissements d'enseignement et de recherche français ou étrangers, des laboratoires publics ou privés.

TITLE: Mechanical alloying and theoretical studies of MnAl(C) magnets

Authors: Van Tang Nguyen[a,b], Florent Calvayrac[a], Anna Bajorek[c,d], Nirina Randrianantoandro[a,*]

[a]*Institut des Molécules et Matériaux du Mans – UMR CNRS n°6283, Le Mans Université, Avenue Olivier Messiaen, 72085 LE MANS Cedex 9.*

[b]*Department of Advanced Materials Science and Nanotechnology, University of Science and Technology of Hanoi, Vietnam Academy of Science and Technology, 18 Hoang Quoc Viet, Hanoi, Vietnam.*

[c]*A. Chełkowski Institute of Physics, University of Silesia in Katowice, Uniwersytecka 4, 40-007 Katowice, Poland.*

[d] *Silesian Center for Education and Interdisciplinary Research, University of Silesia in Katowice, 75 Pułku Piechoty 1A, 41-500 Chorzow, Poland.*

Keywords: MnAl(C) alloys; Ferromagnetic phase; Mechanical alloying; ab initio calculation

Abstract

$Mn_{55}Al_{45}$, $Mn_{55}Al_{44}C_1$, $Mn_{52.2}Al_{45.8}C_2$ and $Mn_{54.2}Al_{43.8}C_2$ were synthesized by the mechanical alloying method. It was the first time that a high purity τ phase up to 99% of weight percentage was obtained in $Mn_{54.2}Al_{43.8}C_2$, which gave the highest saturation magnetization M_s = 570 kAm^{-1} ever reported by mechanical alloying method up to date. The crystallite size of the τ phase of MnAl(C) alloy decreased with increasing carbon doping, varying from 79 to 159 nm. Additionally, the coercivity (H_c) was found to be inversely proportional to the crystallite size of τ phase. Effect of doping carbon and its position in the τ phase of MnAl(C) alloy were also investigated for the first time by first-principle calculations. It was found that by inserting carbon at the interstitial site in the tetragonal structure, a strong stabilization effect and an expansion of unit cell were observed, which are in good agreement with the experimental results. Moreover, our results indicate that carbon doping reduces the magnetic moment of Mn.

1. Introduction

Among the rare-earth-free magnets that are currently being investigated, the manganese aluminum (MnAl) alloy that was first reported by Kono [1] and Koch *et al.* [2] is increasingly gaining attention as having promising intrinsic properties: saturation magnetization $\mu_0 M_S$ = 0.75 T, anisotropy constant K_1 = 1.7 MJm^{-3}, Curie temperature T_c = 650 K, and theoretical energy product $(BH)_{max}$ = 112 kJm^{-3} [3, 4]. Moreover, the MnAl alloy displays good machinability and high corrosion resistance; meanwhile, the elements Mn and Al are highly abundant on earth.

The ferromagnetic properties of the MnAl magnet come from its τ phase, a tetragonal crystallographic structure ($L1_0$) that is formed in a region ranging from 50 to 60 atomic percent (at.%) Mn (**Fig. 1**). However, one of the challenges of obtaining a pure τ phase is that it is metastable, and therefore easily decomposes into two stables phases, the non-magnetic γ_2-Mn_5Al_8 and the β-Mn phase. The τ-phase can be obtained by transformation from the high-temperature ε-phase through a proper cooling from high temperature or annealing at 400-600°C [1, 5]. Doping with a third element in order to improve the stability and magnetic properties of τ phase was reported in many previous works, and carbon (C) has been so far proved to be the best candidate [6-10].

Several attempts were reported in the literature for obtaining a pure τ- phase using many methods: melt spinning, gas atomizing, rapid solidification processing, arc melting, ball milling, drop

synthesis and mechanical alloying. Among those methods, very high purity τ phase was obtained by Q. Zeng et al. by arc-melting [8, 18] and by M. J. Lucis *et al.* by melt spinning [14]. They obtained respectively M_s and H_C values of the order of 650 kAm^{-1} and $H_c \approx 398$ kAm^{-1} for the first and 408 kAm^{-1} and $H_c \approx 75$ kAm^{-1} for the second.

Mechanical alloying, in particular, presents the advantage of producing a nanocrystalline structure with a crystallite size of few nanometers that helps to improve performance of magnetic materials. The best magnetic properties obtained with this method were reported by D.C Crew *et al*., M_s = 442 kAm^{-1}, M_r = 203 kAm^{-1}, H_c = 271 kAm^{-1}, and $(BH)_{max}$ = 10.3 kJm^{-3} [21] but the mechanically alloyed $Mn_{53.1}Al_{43.1}C_{3.8}$ is not pure and contains a secondary phase β-Mn. This is due to a large difference in melting temperature between Mn (1246°C) and Al (660°C), a complicated phase diagram, metastability of the τ phase, as well as many other factors which influence the milling process like milling time, speed, balls-to-powder-weight ratio. Hence, optimization of the mechanical alloying condition, leading to improvement of τ phase content and magnetic properties, is desirable.

The magnetic moment of Mn in the $L1_0$ structure and the magnetic behavior in dependence with the unit cell parameters, electronic structure and magneto-crystalline anisotropy of MnAl alloy were theoretically calculated by A. Sakuma *et al.* and J. Z. Wei *et al.* [18, 26]. As C doping helps to stabilize the τ phase, understanding its position in the structure, and consequently the mechanism of the effect is needed. Indeed, the effect of carbon on stabilizing the τ phase and the position of carbon in the structure were experimentally examined by [27-30]. In detail, an attempt to study the position of C in the τ phase of MnAl(C) magnet by X ray Diffraction was carried out by K. H. Han *et al.*, in which, it was proposed that C should enter the octahedral interstitial sublattice sites at (½;½;0) positions, lying in the Mn atom layers [30]. Neutron diffraction was also employed by Y.c. Yang *et al.*, who found that C would prefer to occupy the (½;½;½) site [27]. However, C.T. Lee *et al.* [29] later on experimentally showed that the c axis increased markedly with the C content as an evidence that C should dissolve interstitially in the bct lattice. With many results from experimental, a further investigation by ab initio studies is necessary.

In order to obtain a pure τ phase and according to the Mn-Al phase diagram (Figure. 1) we prepared by mechanical alloying method several $(Mn_xAl_{100-x})_{100-y}C_y$ alloys where x is the Mn atomic content in the range of 50 to 56 and y is the C atomic content. In the present work, we report our better MnAl(C) alloys with a high purity τ phase, using the mechanical alloying method with a short milling time and adequate heat treatment, as well as a study of the effects and position of C doping, both experimentally and theoretically.

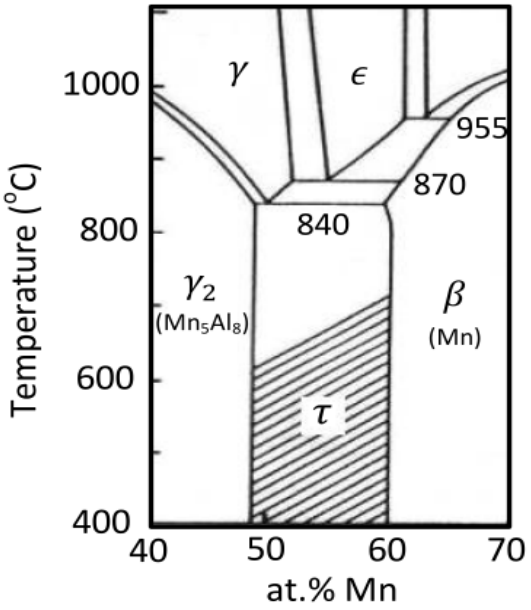


Fig. 1. Phase diagram of MnAl alloys [31].

2. Materials and methods

The manganese (99.95% in purity), aluminum (99.5 % in purity), and carbon (99.95% in purity) powders were weighted and mixed for mechanical alloying. In order to obtain a pure τ phase, the compositions were refined step by step based on the results of previous experiments. Finally, four nominal compositions: $Mn_{52}Al_{48}$, $Mn_{51}Al_{48}C_1$, $Mn_{50}Al_{48}C_2$, and $Mn_{50.5}Al_{47.5}C_2$ were made. Each mixed powder corresponding to each composition was poured into two cylindrical tungsten carbide vials of a planetary ball mill (PULVERISETTE 7 premium line). Then, the two vials were sealed under argon atmosphere in order to avoid oxidation during the milling process. The total milling time of each sample was 10h at a speed of 400 rpm, during which, every 3 minutes, milling was interrupted by a pause of 2 minutes in order to avoid a high temperature arising inside the vials. The balls to powder weight ratio is 50:1.

In order to avoid oxidation, all samples were sealed in a quartz tube vacuumed at 10^{-4} Torr. These samples were then annealed at 1050° C for 1 hour, quenched in water, and finally aged at 500 – 535 °C for 45 minutes to obtain the ε and τ phases, respectively. The ε-to-τ-transformation-temperature was determined by using the Differential Scanning Calorimetry (DSC) technique. The phase identification and microstructure of MnAl(C) alloys was investigated by PANalytical –X ray diffractometer using CuK_α radiation. The compositions and morphology of MnAl(C) samples were examined by Energy Dispersive Spectroscopy (EDS) and Scanning Electron Microscope (SEM). Finally, the magnetic measurements were carried out by Superconducting Quantum Interference Devices (SQUID) MPMS XL7 Quantum Design magnetometer at room temperature and up to external induction field of $B_{ext} = \mu_0 H_{ext} = 7$ T.

A theoretical study of MnAl(C) magnet was carried out using the Quantum Expresso (QE) package (Quantum-opEn-Source Package for Research in Electronic Structure, Simulation, and Optimization, which contains the core package Plane-Wave Self-Consistent Field (PWscf program) using density functional theory (DFT), Plane-Wave (PW) basis set and pseudopotentials [32]. Structural

optimization was performed with a variable cell (Vc-relax) and the spin degree of freedom enabled. Supercells of 100 atoms with or without carbon doping were built starting from ideal structure taken from the Crystallography Open Database COD [33]. Kinetic energy cutoff for wavefunctions (ecutwfc) and for charge density and potential (ecutrho) were set to be 20 Ry and 160 Ry, respectively, after a compromise for speed and accuracy was searched. All ultrasoft pseudopotentials of Mn, Al and C were taken from the QE website, using the PBE density functional [34]. The energy convergence was set to 10^{-4} Ry.

Table 1. Compositions of MnAl(C) compounds before and after 10h of milling estimated by EDS (assuming that the C content is fixed).

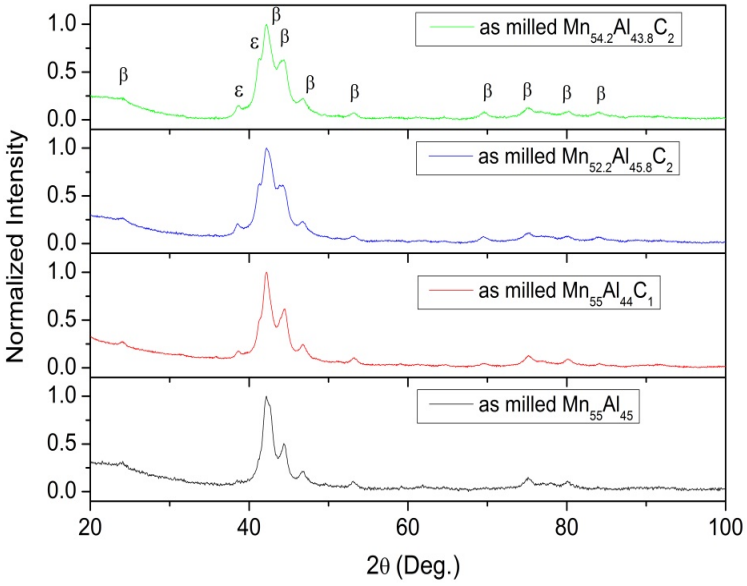
Nominal compositions	After 10h of milling
$Mn_{52}Al_{48}$	$Mn_{55}Al_{45}$
$Mn_{51}Al_{48}C_1$	$Mn_{55}Al_{44}C_1$
$Mn_{50}Al_{48}C_2$	$Mn_{52.2}Al_{45.8}C_2$
$Mn_{50.5}Al_{47.5}C_2$	$Mn_{54.2}Al_{43.8}C_2$

Nominal compositions	After 10h of milling		
	Mn	Al	C
$Mn_{52}Al_{48}$	55 ± 1	45 ± 1	
$Mn_{51}Al_{48}C_1$	55 ± 1	44 ± 1	1
$Mn_{50}Al_{48}C_2$	52 ± 1	46 ± 1	2
$Mn_{50.5}Al_{47.5}C_2$	54 ± 1	44 ± 1	2

3. Results and discussion

3.1. Microstructures

Table 1 shows the compositions of MnAl(C) before and after 10h of milling estimated by EDS technique; in which, only Mn and Al contents were measured while the C amount was assumed to be unchanged after milling. This comes from the fact that the number of electrons in carbon atoms is low and thus the corresponding content is hard to measure accurately by the EDS technique. Mn and Al contents values are given with an accuracy of 2%. As can be seen, there was a slight change in compositions after milling, in which the contents of Mn increased at the expense of Al reduction. The long time recording XRD measurements show neither trace of Al_2O_3 nor unalloyed elements, Mn or Al (**Fig. 2**). The loss of Al during the ball milling process was already observed by chemical analysis of as-milled $Mn_{49.2}Al_{50.8}$ powders where the Al content of the final product decreased when the milling time increased [23]. In addition, J. Eckert *et al.* showed that during the study of glass-forming range in mechanically alloyed Ni-Zr, the overall temperature inside the vial could reach a temperature of 400°C in which the local temperature of the milled $Ni_{70}Zr_{30}$ powders was estimated about 200°C [35]. On the basis of the reasons given above and taking into account the fact that there is a large difference in melting temperature between Mn and Al, we assume that the quantity of Al missing in the as-milled samples is probably deposited on the surface of the balls or on the wall of the vials. This is opposite to the arc melting method that often vaporizes some amount of Mn under a high temperature arc, resulting in the loss of an amount of manganese [8, 19].



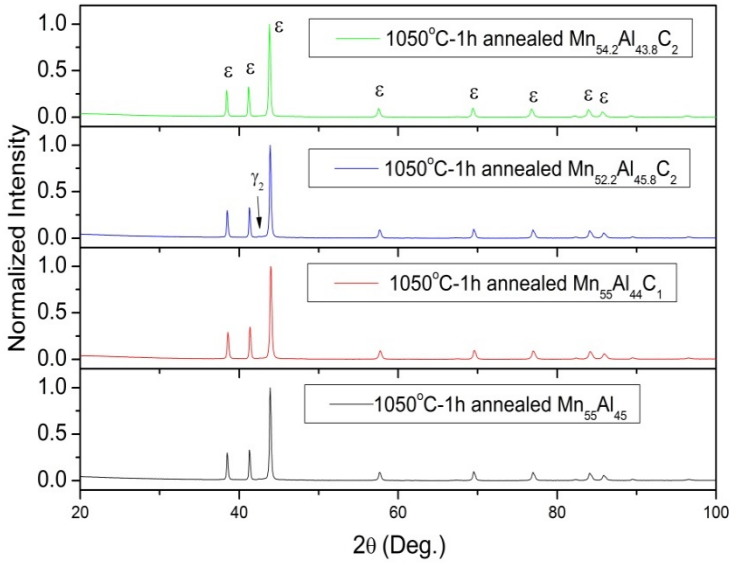


Fig. 2. XRD patterns of (a) "as milled" and (b) MnAl(C) alloys annealed at 1050 °C for 1h and quenched in water.

As can be seen, **Fig. 2(a)** depicts the XRD diagrams of "as milled" and $Mn_{55}Al_{45}$, $Mn_{55}Al_{44}C_1$, $Mn_{52.2}Al_{45.8}C_2$, $Mn_{54.2}Al_{43.8}C_2$ alloys. The broadened of Bragg peaks of the "as milled" sample indicates the presence of a poorly crystallized phase and identified as a mixing of β-Mn and high-temperature ε phases. This "as milled" structure results from the fracturing and cold-welding processes that occurred repeatedly during the milling process. Annealing of "as milled" samples at 1050°C during 1h allowed the phase transformation of the β to the ε phase. **Fig. 2(b)** shows that a very high purity ε phase was observed for the three samples $Mn_{55}Al_{45}$, $Mn_{55}Al_{44}C_1$, and $Mn_{54.2}Al_{43.8}C_2$, but in the $Mn_{52.2}Al_{45.8}C_2$ sample a small amount of γ_2 phase appeared. The appearance of this secondary phase is due to the lower content of Mn, which is close to the γ_2 region (**Fig. 1**).

The DSC curves for determination of ε-to-τ-transformation-temperature were depicted in **Fig. 3**. The T_{peak} is the temperature where half of the transformation was accomplished. The aging temperature was chosen so that whole transformation would be achieved. Hence, the annealed samples were aged at various temperatures ranging from 500 to 535°C for 45 minutes to transform the ε to the τ phase.

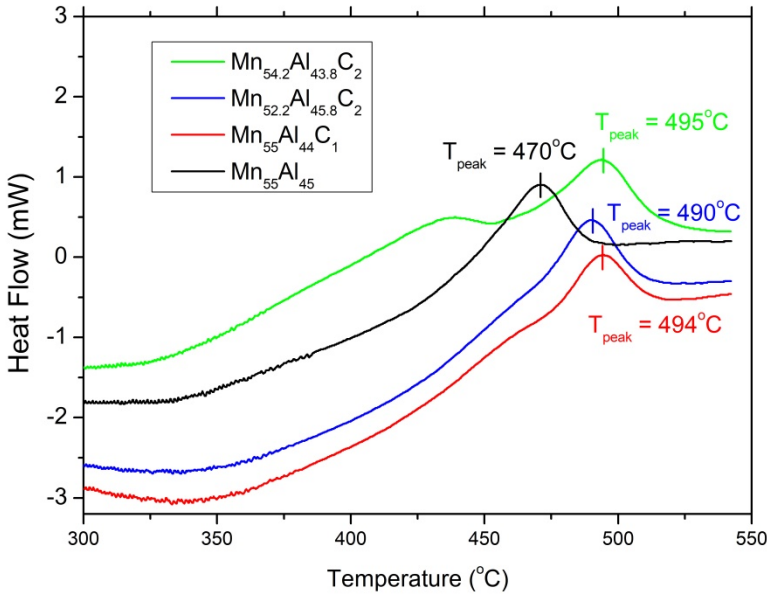


Fig. 3. DSC curves of 1050 °C-1h annealed MnAl(C) alloys for determination of ε-to-τ-transformation-temperature.

XRD patterns of those aged samples are shown in **Fig. 4**. As can be seen, the τ phase was formed in all samples. The highest purity was obtained with the $Mn_{54.2}Al_{43.8}C_2$ alloy, while the β phase appeared in $Mn_{55}Al_{45}$, $Mn_{55}Al_{44}C_1$ and γ_2 phase in $Mn_{52.2}Al_{45.8}C_2$. Identification of phases, [ε (PDF file: 00-011-0416, crystal system: hexagonal, space group: P63/mmcE, space group number: 194), τ (PDF file: 00-030-0028, crystal system: tetragonal, space group: P4/mmm, space group number: 123), β (PDF file: 00-048-1568, crystal system: cubic, space group: P4132, space group number: 213), γ_2 (PDF file: 00-018-0035, crystal system: Rhombohedral, space group: R3m, space group number: 160)], present in each step of the process was done with HighScore Plus Software [36] and the Rietveld refinement of XRD data and determination of microstructure (grain size and phase content) were performed with MAUD program [37]. Crystallographic Information Framework (CIF) files of ε, τ, β, and γ_2 phases used for Rietveld refinement were downloaded from COD [http://www.crystallography.net]. The refined parameters values are presented in **Table 2**. Notice that a good refinement is obtained when Rw < 15.0 and Sig < 2.0.

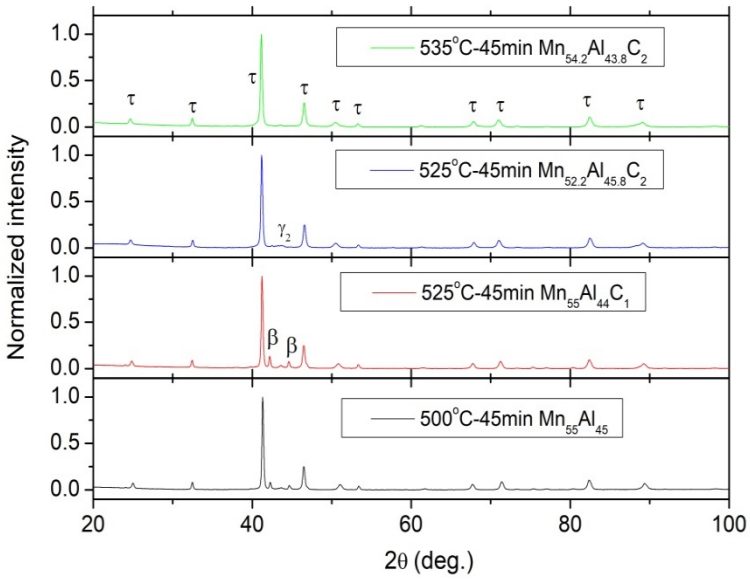


Fig. 4. XRD parterns of MnAl(C) alloys aged at various temperatures from 500 °C to 535 °C for 45 minutes

Examples of the Rietveld refinement of annealed and aged $Mn_{54.2}Al_{43.8}C_2$ are shown in **Fig. 5**.

From table 2, it is shown that the a and c cell parameters of the ε-phase with hexagonal close-packed (hcp) structure increase with carbon content. In the τ-phase with bct structure, cell parameter c possesses the same behavior while the cell parameter adecreases slightly. Therefore, for both structures, an increase of cell volume was observed, indicating that the carbon atoms occupy interstitial sites. This is consistent with the results of ab initio calculation, which predicts that the tetragonal τ-phase is more stabilized when doping C atoms occupy interstitial positions (see Table 4). For the MnAl τ-phase, according to the hole size consideration, among the four nonequivalent octahedral-type interstitial sites only two nonequivalent sites lying in the c-direction have sufficient space to accommodate the C atoms; type I (1/2, 1/2, 0) and type II (0, 0, 1/2) [29]. Otherwise, our results are in agreement with those obtained by different studies in the literature [8, 18, 29] and notably the case of martensite, in which the c axis was elongated while the a axis was slightly reduced since carbon atoms were inserted into the interstitial site of its body center tetragonal (bct) structure [39]. Another example is that reported bt C.T. Lee *et al* [29] from rapidly solidified and heat treated $(Mn_{0.53}Al_{0.47})_{100-x}C_x$ alloys, where the cell volume of pseudo-binary MnAl bct structure increases with C atoms content and in which C doping atoms occupy interstitial sites type I. This is different from the assumption used for our Ab-initio calculation since we considered the interstitial sites type II.

From **Table 2** , it is shown that the crystallite size of the ε phase ranges from 100 to 120 nm. Moreover, after the phase transformation from ε to τ the crystallite size increased slightly for the free and low carbon content samples while it decreased significantly for the samples with higher carbon content.

This is understandable considering the mechanism of nucleation and grain growth during eps-tau transformation and the role of point defects in this process. In such process, presence of defects hampers grains growth and limits their size. This effect of point defects was reported by F. Lemke et al, in which Fe doping suppressed the grain growth of SrTiO3.[38]. For our samples, as carbon atoms were inserted, the defect concentration will increase with increasing amount of carbon. Therefore, a smaller crystallite size with higher carbon concentration would be expected.

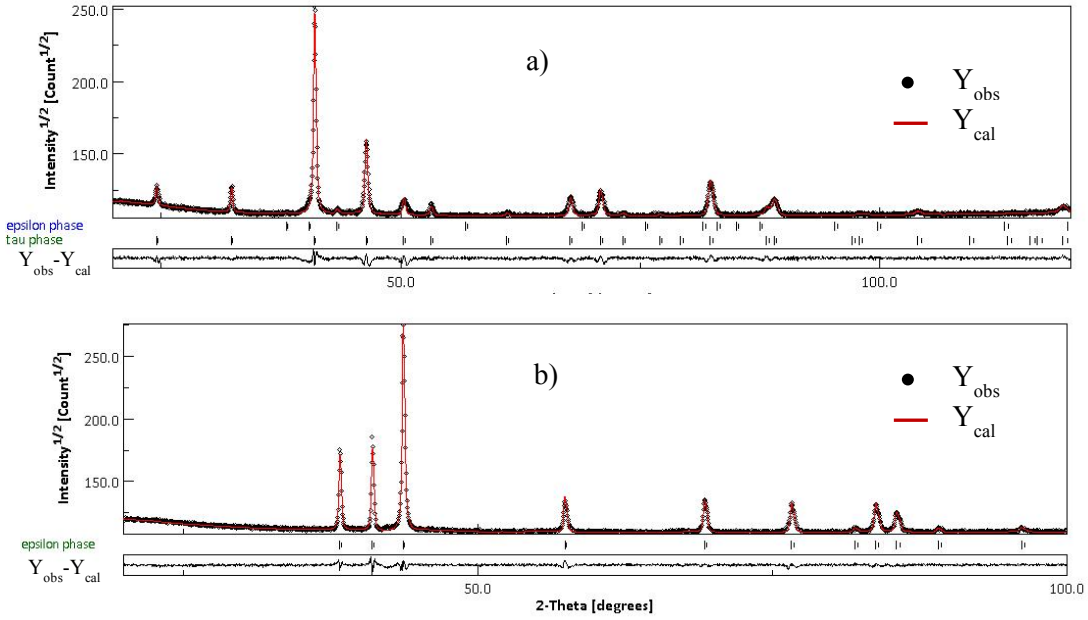


Fig. 5. Rietveld refinement of annealed (a) and aged $Mn_{54.2}Al_{43.8}C_2$ (b) shows the observed data (Y_{obs}), calculated data (Y_{cal}) and also the Y_{obs}-Y_{cal} plot.

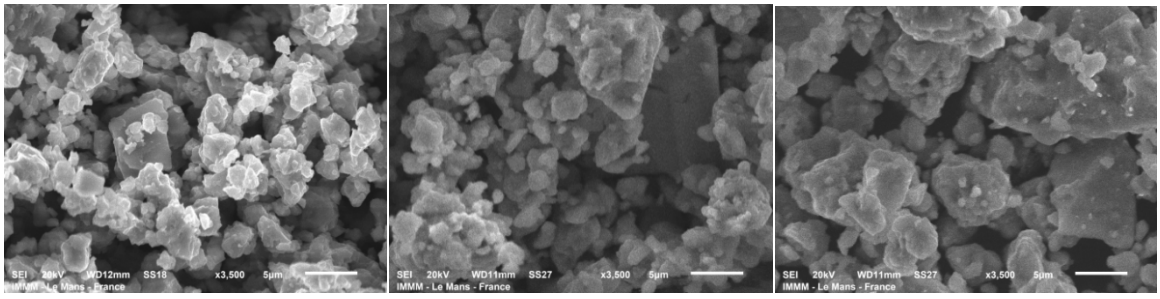
Table 2. Refined microstructure of MnAl(C) alloys.

	ε-phase				τ-phase				
	CS (nm)	a (Å)	c (Å)	Sig - Rwp	CS (nm)	a (Å)	c (Å)	Sig - Rwp	**WP (%)**
$Mn_{55}Al_{45}$	**118**	2.7072 ±0.0001	4.3825 ±0.0001	1.63-1.45	**159**	**2.7742** ±0.0001	**3.5911** ±0.0002	1.87-1.66	**92**
$Mn_{55}Al_{44}C_1$	**102**	2.7084 ±0.0001	4.3865 ±0.0002	1.51-1.35	**137**	**2.7708** ±0.0001	**3.6019** ±0.0002	2.05-1.65	**88**
$Mn_{52.2}Al_{45.8}C_2$	**122**	2.7118 ±0.0001	4.3924 ±0.0001	1.36-1.91	**98**	**2.7675** ±0.0002	**3.6253** ±0.0004	1.48-2.54	**91**
$Mn_{54.2}Al_{43.8}C_2$	**112**	2.7107 ±0.0021	4.4392 ±0.0012	1.59-1.40	**79**	**2.7661** ±0.0002	**3.6245** ±0.0003	1.99-1.79	**99**

CS: Crystallite size.
WP: Weight percentage.

Doping with one carbon in atomic percentage, as in the case of $Mn_{55}Al_{44}C_1$, seems to have no effect on stabilizing the tetragonal structure as the β phase still exists with a comparable amount with the free carbon sample, $Mn_{55}Al_{45}$. This indicates that stabilizing the τ phase by C insertion in the tetragonal structure needs a certain threshold of C content and according to our results this is higher than 1%.

Fig. 6 shows SEM images of $Mn_{54.2}Al_{43.8}C_2$ powders at 3500 times of magnification in which one can observe the morphology evolution of powders from the as-milled state and after heat treatment and aging processes. For the as-milled powders (**Fig. 6**. (a)) it can be seen a wide particle size distribution with an average size in order of 3±1μm. **Fig. 6**. (b) shows the evolution after annealing at 1050°C/1h and quenched in water the as-milled sample. This treatment aims at forming the high temperature ε-phase. The overall particle size did not evolve in great proportions compared to that of as-milled powder. **Fig. 6**. (c) shows particles powder morphology after aging the heat treated sample at 535°C/45 min to realize the phase transformation ε→τ. It is shown that particles size increase substantially and can reach the value of 20μm. Indeed, the change in particles size especially concerns the low size particles for which the provided thermal energy produces a successive coalescence, germination and growth processes, which allow for an increase of their overall size. In a previous work related to the phase transition from γ-Fe2O3 to α-Fe2O3 nanoparticles induced by thermal treatment and laser irradiation we have already observed this phenomenon [40].



a) b) c)

Fig. 6. SEM images $Mn_{54.2}Al_{43.8}C_2$ a) after 10h of milling, b) after annealed at 1050 °C -1h and c) after aged at 535 °C-45 minutes.

3.2. **Magnetic properties**

Magnetic properties of the ε phase of annealed $Mn_{54.2}Al_{43.8}C_2$ at room temperature was investigated by recording the external magnetic field dependence of magnetization M(H). The result is shown in **Fig. 7**, where one can observe a linear dependence of magnetization as a function of the external magnetic field with no hysteresis as the indication of paramagnetic characteristics. In combination with XRD, it confirms the high purity of the ε phase obtained in annealed $Mn_{54.2}Al_{43.8}C_2$. However, it is well known that ε is antiferromagnetic with a Néel temperature $T_N = 97$ K [41].

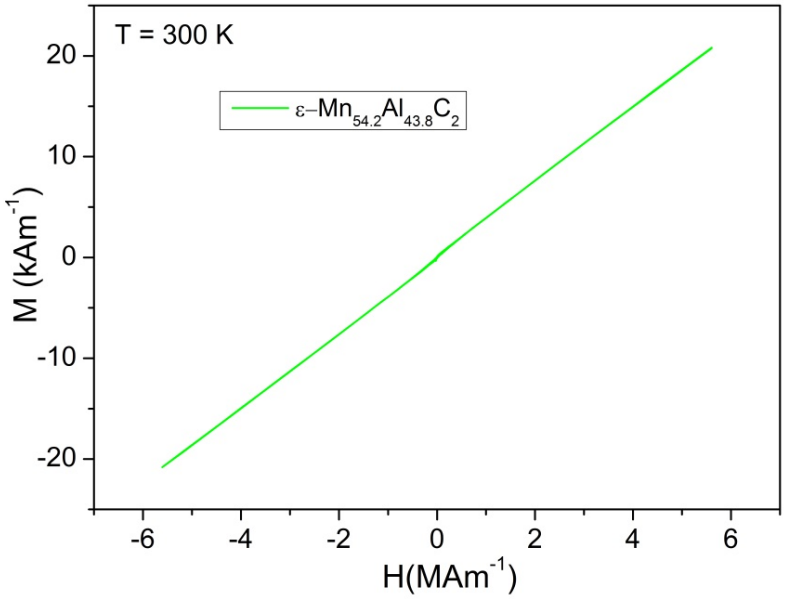


Fig. 7. Magnetic field dependence M(H) of ε - $Mn_{54.2}Al_{43.8}C_2$ measured at room temperature.

Room temperature M(H) hysteresis loops of all aged samples are shown in **Fig. 8**. Both secondary phases, γ_2-Mn_5Al_8 and the β-Mn are paramagnetic at room temperature, therefore, their contributions to the M(H) curves of mostly ferromagnetic material (τ-phase) are negligible. The inset figure represents a larger scale view of the center area of M(H) curves. As one can see, magnetizations of all aged samples were almost saturated under an external magnetic field (H) of 5.5 MAm^{-1}. The hysteresis loops indicate that all samples are ferromagnetic and originated from the τ phase. Magnetic properties values related to carbon content are also presented in **Table 3.**

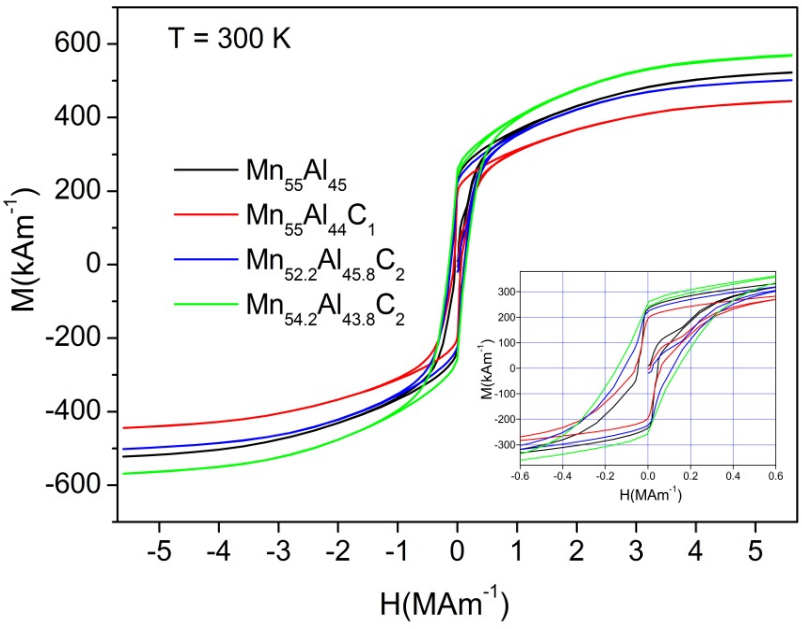


Fig. 8. Hysteresis loops of aged MnAl(C) alloys at room temperature.

The mass density of τ phases, ρ=5.1 g/cm^3, which came from the refinement data, was used to calculate the energy product $(BH)_{max}$. As can be seen, the coercivity (H_c) increased monotonically with increasing carbon content. In detail, H_c of $Mn_{54.2}Al_{43.8}C_2$ has the highest value of 143 kAm^{-1} while that of free-doped carbon $Mn_{55}Al_{45}$ has the lowest, with 46.3 kAm^{-1}. Our values are smaller than those originating from samples obtained by the same technique reported by D.C. Crew *et al.*, where the highest obtained H_c value was of 271 kAm^{-1} with 1.1 wt.% C doping [21] or by O. Obi *et al.*, with H_c = 175 kAm^{-1} at 1% C doping [22]. This difference may come from the higher crystallite size value of our samples compared to others. For example, crystallite size of τ phase reported by O. Obi *et al.* was 39 nm [22] compared to 79 nm of $Mn_{54.2}Al_{43.8}C_2$ in our work. According to J.M.D. Coey [42], the maximum radius of a spherical particle that is a single domain in equilibrium R_{sd} is calculated by:

$$R_{sd} = 36\frac{\sqrt{|K_1|A}}{\mu_o M_s^2} \quad (1)$$

where K_1, A, μ_o, M_s are the uniaxial anisotropy constant, the exchange stiffness, the vacuum permeability, and the saturation magnetization, respectively. Substituting the parameters of MnAl alloy, in which K_1= 1.7 MJm^{-3} [4], $A \approx 10^{-11}$ Jm^{-1}, and $M_s = 0.57$ MAm^{-1}, gives $R_{sd} \approx 330$ nm or 660 nm in diameter. This value is comparable with the reported diameter of single domain of 773 nm by [43] and 710 nm by [44]. The calculated value 660 nm is higher than the experimentally obtained crystallite size (79 – 159 nm) of aged samples in our work, suggesting that the crystallites of these aged samples are in the single domain region. The obtained coercive field values decrease when the crystallite size increases. **Fig. 9** exhibits a linear dependence of coercive field as a function of the inverse of crystallite size. At this stage, it is important to emphasize that the microstructure of powders obtained by ball milling consists of a crystallized grains separated by grain boundaries [45, 46]. As mentioned previously, it results from the fracturing and cold-welding processes that occurred repeatedly during the milling process.

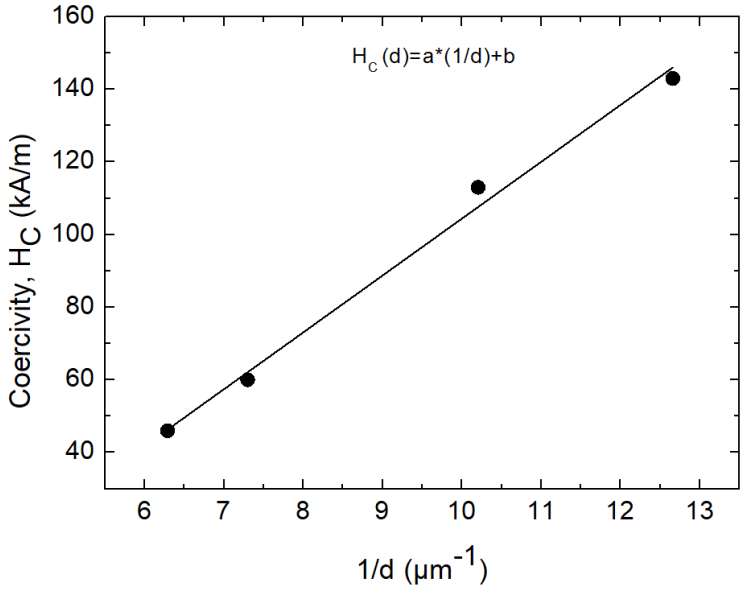


Fig. 9. Crystallite size dependence of coercivity (Hc)
(•) represent the experimental data and the line (—) the linear fit.

For our samples, the grains or crystallites are a few tens of nanometers while the individual particles can reach a few micrometers as showing by the SEM images **(Fig. 6. a, b and c)**. Based on to the measured grain size values, the studied particles are constituted of single magnetic domains delimited

by grain boundaries. The grain size dependence of coercivity and permeability (GSDCP) theory was developed by A. Mager [47] and then by G. Herzer [48-50], D. Xue *et al.* [51], and F. Pfeifer *et al.* [52]. Indeed, if the grain size exceeds the domain wall width,

$$\delta = \pi \sqrt{\frac{A}{K_1}} \quad (2)$$

the magnetization process is determined by the domain wall pinning at the grain boundaries, in that case, a linear dependence of the coercive field (H_c) as a function of the inverse of crystallite size (d) is predicted [48], such as:

$$H_C \approx p_c \frac{\sqrt{AK_1}}{\mu_0 M_s d} \quad (3)$$

where the pre-factor p_c is typically of order of 6 or 3 for 180° or 90° domain walls in an assembly of randomly oriented cubic particles. According to the magnetic parameter values of τ phase, δ ≈ 8 nm, and the linear fit of the curve $H_C(1/d)$ gives a value of $p_c \approx 2.8$. This value is in agreement with the theoretical value, $p_c = 3$, predicted by A. Mager [47] and G. Herzer [48].

Saturation magnetization M_s displayed a similar trend as H_c, except for a minimum value found at $Mn_{55}Al_{44}C_1$ (**Table 3**). This behavior can be explained by corresponding to the τ phase content in each sample, in which, $Mn_{55}Al_{44}C_1$ has the lowest amount at 88% and $Mn_{54.2}Al_{43.8}C_2$ has the highest at 99%. This is because of the carbon doping effect that stabilizes the τ phase, increases its content in the sample volume and improves the magnetic properties, by increasing M_s, M_r and $(BH)_{max}$ values. One can see that $Mn_{54.2}Al_{43.8}C_2$ has the best performance with $M_s = 570$ kAm^{-1} (111.78 emu/g), $M_r = 255$ kAm^{-1} (50 emu/g), and $(BH)_{max} = 7.8$ kJ/m^3 (**Table 3**). **Table 3** also lists the magnetic properties values obtained by other authors using the same synthesis technique ([9, 21, 22]) in comparison with those of our samples. One can emphasize that the M_s and M_r values of our $Mn_{54.2}Al_{43.8}C_2$ mechanically alloyed powder are the highest values ever reported by the mechanical alloying technique up to date. This high value is due to the high purity of τ phase in aged $Mn_{54.2}Al_{43.8}C_2$. The M_s in our work is smaller than bulk $Mn_{54}Al_{46}$ synthesized by arc melting [8, 18], comparable with $(Mn_{55}Al_{45})_{100}C_2$ obtained by drop synthesis [20], and remarkably higher than $Mn_{54}Al_{46}$ by gas atomization method [11], and $Mn_{55}Al_{45}$ by melt spinning [16]. However, a low $(BH)_{max}$ was still obtained, which mainly comes from the low H_c.

Table 3. Comparison of magnetic properties with other results also synthesized by mechanical alloying.

Samples	M_s (kAm^{-1})	M_r (kAm^{-1})	H_c (kAm^{-1})	$(BH)_{max}$ (kJ/m^3)	Reference
$Mn_{53.1}Al_{43.1}C_{3.8}$	442	203	271	10.3	[21]
$Mn_{53}Al_{47}$	296	158	103	3.6	[22]
$Mn_{55}Al_{45}$	336	102	80	Unknown	[9]
$Mn_{55}Al_{45}$	**523 ± 0.3**	**230 ± 3**	**46 ± 0.9**	**4.0 ± 0.1**	**In our work**
$Mn_{55}Al_{44}C_1$	**444 ± 0.5**	**194 ± 1**	**60 ± 0.1**	**2.8 ± 0.1**	
$Mn_{52.2}Al_{45.8}C_2$	**501± 0.3**	**219 ± 3**	**113 ± 0.2**	**5.0 ± 0.1**	
$Mn_{54.2}Al_{43.8}C_2$	**570 ± 0.5**	**255 ± 2**	**143 ± 4.0**	**7.8 ± 0.1**	

4. Ab initio studies

In order to study the position of carbon atoms in the case of doping and their effect on the stabilization of τ phase, supercells of 100 atoms ($Mn_{50}Al_{50}$) with tetragonal structure were constructed with or without carbon doping. The dimension of the supercell is (5a x 5a x 2c), where a and c are the

axis of the primitive cell. Carbon was inserted up to two carbons atoms for one supercell, with two examples: firstly, at the interstitial position (0;0;½) and secondly with a substitution of Al atoms at (½; ½; ½). The reason that carbon was inserted at (0;0;½) is because the c axis is increased when carbon is added (**Table 2**), and C experiences the largest space surrounded by the two closest Mn and four other Al atoms nearby in the supercell. Total energy (E_{total}), optimized structure, and the resulting magnetization were computed in each case. The results are summarized in **Table 4**.

It can be seen that the total energy after full structural optimization was reduced when carbon was added at interstitial site (0;0;½) where E_{total} decreased from 11.14 Ry and 22.29 Ry with one and two carbons adoption, respectively. This means that the tetragonal structure was stabilized under doping of carbon at the interstitial sites. In contrast, E_{total} increased when Al was substituted by carbon, no matter if one or two carbons were added. The more carbon atoms were substituted, the higher E_{total} was found. This can be easily seen by the value ΔE_{total}, namely, the difference in energy between a system without added carbon E_o and with added carbon E_c. The changes in supercell volume $\Delta V/V_o(\%)$ between the volume V_o of the pure system and the volume V_c of the carbon doped system show a good agreement with empirical data in case of interstitial doping. In detail, $V_{supercell}$ increased with the addition of carbon. On the other hand, $V_{supercell}$ was contracted when C was added at (½; ½; ½) site. The lattice parameters of a and c axis after optimization are also presented in the **Table 4**. These values are smaller than the reported valued in **Table 2**. This can be understood since those values are calculated at 0 K. One can see that both a and c axes expand when carbon is interstitially inserted except for the case of the c axis when one carbon is added. Reduction of all a and c axis are observed in the case of carbon substitution. As mentioned above, the structure of τ phase may include the distortion as in case of martensite where internal stress exists, for both τ phase and martensite are metastable. Meanwhile, in the calculation of cell optimization, the atom positions are optimized so that the internal stress is minimized. So, for the case of interstitial insertion, the increase or decrease of a axis and c axis could be observed, yet there was a total gain in the volume.

Absolute magnetization, which is mainly contributed by the ferromagnetic coupling between Mn atoms, and effective magnetic moment μ_{eff} of Mn was found to be notably reduced as more carbon was added at interstitial sites, while there was only a slight decline in case of substitution. This observation is in opposition with the report by J. Z. Wei *et al.* that was obtained from neutron diffraction analysis [18]. However, the decline of magnetization with carbon doping was also reported by Q. Zeng *et al.* [8], and J. Z. Wei *et al.* [18]. On the other hand, O. Moze *et al.* [10] and L. Pareti *et al.* [53] reported an increase of M_s when carbon was doped; however, although M_s also depends on the τ phase content of each sample, that was not mentioned in these two articles. Indeed, in our work, the τ phase content in aged $Mn_{55}Al_{45}$ (92%) is comparable with aged $Mn_{52.2}Al_{45.8}C_2$ (91%), but possesses notably higher M_s (**Table 3**). The reduction of magnetization when carbon is added could be explained based on the change of Curie temperature (T_c). Indeed, the T_c depends on the exchange energy as below:

According to B. D. Cullity [54], the exchange energy E_{ex} between one atom and the nearest surrounding atoms with the same and parallel spin is defined as:

$$E_{ex} = z(-2J_{ex}S^2) \quad (4)$$

where z, J_{ex}, and S are the coordination number, the exchange integral and the total spin, respectively. In this equation, the exchange integral J_{ex} is proportional to T_c according to [54]:

$$J_{ex} = \frac{3k_B T_c}{2zS(S+1)} \quad (5)$$

where k_B is the Boltzmann constant.

It was reported in the literature that T_c decreases with the addition of carbon [18, 53]; therefore, according to the formula (4), resulting in decreasing the exchange integral J_{ex} between Mn atoms, and consequently the reduction of the magnetization as well.

The μ_{eff_cal} of Mn at (0;0;0) site of $Mn_{50}Al_{50}$ in our work is found at 2.24 μ_B which is smaller than that by J. Z. Wei *et al.* [18], which $\mu_{_cal} = 2.44\ \mu_B$, and by A. Sakuma [26], which $\mu_{_cal} = 2.4\ \mu_B$. The difference may come from the difference in lattice size of $Mn_{50}Al_{50}$ in the calculation, from the accuracy of the calculation itself linked to force and energy convergence, or from the particular theoretical choices we made (DFT, pseudopotentials, discretization, etc).

The experimental effective magnetic moment μ_{eff_ex} of $Mn_{54.2}Al_{43.8}C_2$ was calculated by equation $M_s = \langle n \rangle\ \mu_{eff_ex}$, where <n> is the number of Mn atoms. This gave $\mu_{eff_ex} = 1.56\ \mu_B$ at T = 300 K, meanwhile the calculated effective magnetic moment with 2 C doping at interstitial site was found at the value $\mu_{eff_cal} = 2.08\ \mu_B$ at T = 0 K (**Table 4**), which is in reasonable agreement with the the μ_{eff_ex} at T = 300K.

Table 4. Summary results of modelling MnAl(C) alloys with interstitial and substitution cases.

		Total energy E_{total} (Ry)	ΔE_{total} (Ry) = $E_C - E_o$	Supercell volume V (Å^3)	$\Delta V/V_o$ (%)= $(V_c - V_o)*100/V_o$	a axis (Å)	c axis (Å)	Absolute magnetization (μ_B)	μ_{eff_cal} of Mn (μ_B)
Non carbon		-11081.49	**0**	1062.12	**0**	2.5559	3.2515	112.81	2.24
Interstitial	Add 1 C	-11092.63	**-11.14**	1064.17	**0.19**	2.5586	3.2512	107.29	2.14
	Add 2 C	-11103.78	**-22.29**	1066.16	**0.38**	2.5597	3.2543	104.07	2.08
Substitution	Add 1 C	-11080.27	**1.22**	1058.71	**-0.32**	2.5528	3.2492	112.20	2.24
	Add 2 C	-11079.09	**2.40**	1054.72	**-0.70**	2.5514	3.2400	111.37	2.22

5. Conclusion

Tetragonal MnAl(C) alloys were synthesized by the mechanical alloying method with a short milling time, following by adequate heat treatment. The nominal composition of MnAl(C) was changed after 10h of milling. The microstructure of obtained τ phase powders is constituted of single magnetic

domains crystallites delimited by grain boundaries for which the coercive field increases with the inverse of grain size. This behavior is in agreement with the grain size dependence of coercivity and permeability (GSDCP) theory and therefore indicates that the magnetization process is determined by the domain wall pinning at the grain boundaries. Moreover, the crystallite size of τ phase was found to decrease with the addition of carbon. The mechanical alloyed $Mn_{54.2}Al_{43.8}C_2$ possesses the highest purity of τ phase (99%) after 10h of milling, annealed at 1050 °C for 1h and aged at 535 °C for 45 minutes, having M_s= 570 kAm^{-1}, M_r = 255 kAm^{-1}, H_c= 143 kAm^{-1} and $(BH)_{max}$ = 7.8 kJ/m^3. This M_s is the highest value ever reported by mechanical alloying method.

Both experimental and theoretical studies show the stability enhancement of the τ phase with adoption of carbon. In addition, the results of an ab initio modelling study indicate that carbon should enter the interstitial site. While carbon stabilizes the τ phase, it reduces the magnetic moment of Mn.

6. Acknowledgment

The authors are thankful to Vietnamese Government Scholarship 911 for financial support of the study. CPU hours for the calculations were under GENCI A0010906171 and CRIANN x007 projects.

References

[1] H. Kōno, On the Ferromagnetic Phase in Manganese-Aluminum System, Journal of the Physical Society of Japan, 13 (1958) 1444-1451.
[2] A. J. J. Koch, P. Hokkeling, M. G. v. d. Steeg, K.J.d. Vos, New Material for Permanent Magnets on a Base of Mn and Al, Journal of Applied Physics, 31 (1960) S75-S77.
[3] R. Skomski, J.M.D. Coey, Magnetic anisotropy — How much is enough for a permanent magnet?, Scripta Materialia, 112 (2016) 3-8.
[4] J.M.D. Coey, Permanent magnets: Plugging the gap, Scripta Materialia, 67 (2012) 524-529.
[5] W. Koester, Aufbau und magnetische Eigenshaften der Aluminium-Mangan-Legierungen mit mehr als 25 At.%Mn, Z.Metallk, 51 (1960) 271-280.
[6] S. Mican, D. Benea, R. Hirian, R. Gavrea, O. Isnard, V. Pop, M. Coldea, Structural, electronic and magnetic properties of the Mn50Al46Ni4 alloy, Journal of Magnetism and Magnetic Materials, 401 (2016) 841-847.
[7] Z.W. Liu, C. Chen, Z.G. Zheng, B.H. Tan, R.V. Ramanujan, Phase transitions and hard magnetic properties for rapidly solidified MnAl alloys doped with C, B, and rare earth elements, Journal of Materials Science, 47 (2012) 2333-2338.
[8] Q. Zeng, I. Baker, J.B. Cui, Z.C. Yan, Structural and magnetic properties of nanostructured Mn–Al–C magnetic materials, Journal of Magnetism and Magnetic Materials, 308 (2007) 214-226.
[9] O. Kohmoto, N. Kageyama, Y. Kageyama, H. Haji, M. Uchida, Y. Matsushima, Magnetic properties of mechanically alloyed Mn-Al-C powders, Journal of Physics: Conference Series, 266 (2011) 012016.
[10] O. Moze, L. Pareti, A. Ermakov, Neutron diffraction and magnetic investigations of Ga substituted MnAl permanent magnet materials, Journal of applied physics, 63 (1988) 4616-4619.
[11] C. Anurag, Y. Rumana, B. Ian, A comparison of τ -MnAl particulates produced via different routes, Journal of Physics: Condensed Matter, 26 (2014) 064201.
[12] J. Law, J. Rial, M. Villanueva, N. López, J. Camarero, L. Marshall, J. Blázquez, J. Borrego, V. Franco, A. Conde, Study of phases evolution in high-coercive MnAl powders obtained through short milling time of gas-atomized particles, Journal of Alloys and Compounds, 712 (2017) 373-378.
[13] J. Rial, M. Villanueva, E. Céspedes, N. López, J. Camarero, L. Marshall, L. Lewis, A. Bollero, Application of a novel flash-milling procedure for coercivity development in nanocrystalline MnAl permanent magnet powders, Journal of Physics D: Applied Physics, 50 (2017) 105004.
[14] M.J. Lucis, T.E. Prost, X. Jiang, M. Wang, J.E. Shield, Phase transitions in mechanically milled Mn-Al-C permanent magnets, Metals, 4 (2014) 130-140.

[15] A. Chaturvedi, R. Yaqub, I. Baker, Microstructure and magnetic properties of bulk nanocrystalline MnAl, Metals, 4 (2014) 20-27.
[16] I. Janotová, P. Švec, I. Mat'ko, D. Janičkovič, J. Zigo, M. Mihalkovič, J. Marcin, I. Škorvánek, Phase analysis and structure of rapidly quenched Al-Mn systems, Journal of Alloys and Compounds, 707 (2017) 137-141.
[17] J.H. Huang, P.C. Kuo, Influence of carbon on the phase transformation kinetics and magnetic properties of Mn□Al alloys, Materials Science and Engineering: B, 22 (1994) 256-260.
[18] J. Z. Wei, Z. G. Song, Y. B. Yang, S. Q. Liu, H. L. Du, J. Z. Han, D. Zhou, C. S. Wang, Y. C. Yang, A. Franz, D. Többens, J.B. Yang, τ-MnAl with high coercivity and saturation magnetization, AIP Advances, 4 (2014).
[19] H. Jian, K.P. Skokov, O. Gutfleisch, Microstructure and magnetic properties of Mn–Al–C alloy powders prepared by ball milling, Journal of Alloys and Compounds, 622 (2015) 524-528.
[20] H. Fang, S. Kontos, J. Ångström, J. Cedervall, P. Svedlindh, K. Gunnarsson, M. Sahlberg, Directly obtained τ-phase MnAl, a high performance magnetic material for permanent magnets, Journal of Solid State Chemistry, 237 (2016) 300-306.
[21] D.C. Crew, P.G. McCormick, R. Street, MnAl and MnAlC permanent magnets produced by mechanical alloying, Scripta Metallurgica et Materialia, 32 (1995) 315-318.
[22] O. Obi, L. Burns, Y. Chen, T. Fitchorov, S. Kim, K. Hsu, D. Heiman, L.H. Lewis, V.G. Harris, Magnetic and structural properties of heat-treated high-moment mechanically alloyed MnAlC powders, Journal of Alloys and Compounds, 582 (2014) 598-602.
[23] K.J. Kim, K. Sumiyama, K. Suzuki, Ferromagnetic α-Mn-type Mn□ Al alloys produced by mechanical alloying, Journal of alloys and compounds, 217 (1995) 48-51.
[24] S. Ibrahim, Phase Stability in Mechanically Alloyed Mn-30at.%Al Egypt. J. Solids, 28, No 2 (2005).
[25] T. Saito, Magnetic properties of Mn–Al system alloys produced by mechanical alloying, Journal of applied physics, 93 (2003) 8686-8688.
[26] A. Sakuma, Electronic structure and magnetocrystalline anisotropy energy of MnAl, Journal of the Physical Society of Japan, 63 (1994) 1422-1428.
[27] Y.c. Yang, W.w. Ho, C. Lin, J.l. Yang, H.m. Zhou, J.x. Zhu, X.x. Zeng, B.s. Zhang, L. Jin, Neutron diffraction study of hard magnetic alloy MnAlC, Journal of applied physics, 55 (1984) 2053-2054.
[28] T. Ohtani, N. Kato, S. Kojima, K. Kojima, Y. Sakamoto, I. Konno, M. Tsukahara, T. Kubo, Magnetic properties of Mn-Al-C permanent magnet alloys, IEEE Transactions on Magnetics, 13 (1977) 1328-1330.
[29] C. Lee, K. Han, I. Kook, W. Choo, Phase and lattice parameter relationships in rapidly solidified and heat-treated (Mn 0.53 Al 0.47) 100− x C x pseudo-binary alloys, Journal of materials research, 7 (1992) 1690-1695.
[30] K.H. Han, C.T. Lee, W.K. Choo, On the Position of Carbon Atom in the τ-Phase of Carbon-Doped Mn-Al Permanent Magnets, physica status solidi (a), 136 (1993) 21-28.
[31] A. McAlister, J. Murray, The (Al− Mn) Aluminum-Manganese system, Journal of Phase Equilibria, 8 (1987) 438-447.
[32] G. Paolo, B. Stefano, B. Nicola, C. Matteo, C. Roberto, C. Carlo, C. Davide, L.C. Guido, C. Matteo, D. Ismaila, C. Andrea Dal, G. Stefano de, F. Stefano, F. Guido, G. Ralph, G. Uwe, G. Christos, K. Anton, L. Michele, M.-S. Layla, M. Nicola, M. Francesco, M. Riccardo, P. Stefano, P. Alfredo, P. Lorenzo, S. Carlo, S. Sandro, S. Gabriele, P.S. Ari, S. Alexander, U. Paolo, M.W. Renata, QUANTUM ESPRESSO: a modular and open-source software project for quantum simulations of materials, Journal of Physics: Condensed Matter, 21 (2009) 395502.
[33] S. Gražulis, A. Daškevič, A. Merkys, D. Chateigner, L. Lutterotti, M. Quirós, N.R. Serebryanaya, P. Moeck, R.T. Downs, A. LeBail, "Crystallography Open Database (COD): an open-access collection of crystal structures and platform for world-wide collaboration", Nucleic Acids Research, 40 (2012) D420-D427.
[34] P. Giannozzi, Notes on pseudopotential generation. Scuola Normale Superiore di Pisa, (2007).
[35] J. Eckert, L. Schultz, E. Hellstern, K. Urban, Glass-forming range in mechanically alloyed Ni-Zr and the influence of the milling intensity, Journal of Applied Physics, 64 (1988) 3224-3228.

[36] M.S. T. Degen, E. Bron, U. König, G. Nénert, The HighScore suite, in: Powder Diffraction December 2014, pp. S13-S18.
[37] L. Lutterotti, R. Campostrini, S. Gialanella, R. Di Maggio, Microstructural characterisation of amorphous and nanocrystalline structures through diffraction methods, in: Materials Science Forum, Trans Tech Publ, 2000, pp. 657-664.
[38] F. Lemke, W. Rheinheimer, M.J. Hoffmann, Sintering and grain growth in SrTiO3: impact of defects on kinetics, Journal of the Ceramic Society of Japan, 124 (2016) 346-353.
[39] S. Kalpakjian, S.R. Schmid, Manufacturing engineering and technology, Pearson Upper Saddle River, NJ, USA, 2014.
[40] Y. El Mendili, J.-F.o. Bardeau, N. Randrianantoandro, F. Grasset, J.-M. Greneche, Insights into the mechanism related to the phase transition from γ-Fe2O3 to α-Fe2O3 nanoparticles induced by thermal treatment and laser irradiation, The Journal of Physical Chemistry C, 116 (2012) 23785-23792.
[41] J.J. Wysłocki, P. Pawlik, A. Przybył, Magnetic properties of the non-oriented ε-phase in Mn–Al–C permanent magnet, Materials Chemistry and Physics, 60 (1999) 211-213.
[42] J.M.D. Coey, Magnetism and Magnetic Materials, Cambridge University Press, New York, 2010.
[43] J. Thielsch, F. Bittner, T. Woodcock, Magnetization reversal processes in hot-extruded τ-MnAl-C, Journal of Magnetism and Magnetic Materials, 426 (2017) 25-31.
[44] T. Klemmer, D. Hoydick, H. Okumura, B. Zhang, W. Soffa, Magnetic hardening and coercivity mechanisms in L10 ordered FePd ferromagnets, Scripta Metallurgica et Materialia, 33 (1995) 1793-1805.
[45] D. Zhang, Processing of advanced materials using high-energy mechanical milling, Progress in Materials Science, 49 (2004) 537-560.
[46] E.B. Herbold, J.L. Jordan, N. Thadhani, Effects of processing and powder size on microstructure and reactivity in arrested reactive milled Al+ Ni, Acta Materialia, 59 (2011) 6717-6728.
[47] A. Mager, Über den Einfluß der Korngröße auf die Koerzitivkraft, Annalen der Physik, 446 (1952) 15-16.
[48] G. Herzer, Grain size dependence of coercivity and permeability in nanocrystalline ferromagnets, IEEE Transactions on Magnetics, 26 (1990) 1397-1402.
[49] G. Herzer, Grain structure and magnetism of nanocrystalline ferromagnets, IEEE Transactions on Magnetics, 25 (1989) 3327-3329.
[50] G. Herzer, Soft magnetic nanocrystalline materials, Scripta Metallurgica et Materialia, 33 (1995) 1741-1756.
[51] D. Xue, G. Chai, X. Li, X. Fan, Effects of grain size distribution on coercivity and permeability of ferromagnets, Journal of Magnetism and Magnetic Materials, 320 (2008) 1541-1543.
[52] F. Pfeifer, C. Radeloff, Soft magnetic Ni-Fe and Co-Fe alloys-some physical and metallurgical aspects, Journal of Magnetism and Magnetic Materials, 19 (1980) 190-207.
[53] L. Pareti, F. Bolzoni, F. Leccabue, A.E. Ermakov, Magnetic anisotropy of MnAl and MnAlC permanent magnet materials, American Institute of Physics, 59 (1986) 3824-3828.
[54] B. D. Cullity, C.D. Graham, Introduction to Magnetic Materials, Wiley-IEEE Press, 2008.